Magnetic Field Profiles in Fusion Plasmas in the Presence of Equilibrium Flow.

L. Guazzotto   R. Paccagnella

Consorzio RFX

Associazione ENEA - EURATOM sulla fusione

Corso Stati Uniti 4, I-35127, Padova, Italy

Abstract

In nuclear fusion magnetic confinement devices, equilibrium calculations for realistic systems are necessarily based on numerical solutions. In the present work, we describe some of the latest updates to the code FLOW [L. Guazzotto, R. Betti, J. Manickam and S. Kaye, Phys. of Plasmas **11**, 604 (2004)] and give some applications. In this work we apply the code to both tokamak and Reverse Field Pinch (RFP) configurations. It is shown that plasma rotation can have a non-negligible effect on tokamak resonant modes, such as Neoclassical Tearing Modes, in particular by modifying the location of the resonant surface. Regarding RFPs, we show how toroidal flow reversal (detected in experiments) can be understood as an equilibrium effect, and how neoclassical effect can modify the plasma resistivity and current profiles.

I Introduction.

Among the areas of active research work in the nuclear-fusion, magnetic-confinement field, is the study of equilibrium properties of the magnetic configurations. An accurate equilibrium calculation is the first step in the evaluation of a magnetic confinement device, existing or under development.

The key to achieving successful energy production with magnetic confinement devices is the efficient utilization of the magnetic fields used to confine the plasma. That is quantified with the figure of merit β, the ratio between plasma pressure and magnetic pressure, which is an equilibrium quantity. Even though β is in fact limited by stability rather than equilibrium concerns, an accurate equilibrium calculation is essential, since any stability consideration must necessarily be based on preliminary equilibrium calculations.

In recent times, one specific area of exciting development for equilibrium calculations was the inclusion of equilibrium rotation in the models. In the first decades of tokamak research, plasma rotation was commonly neglected in equilibrium calculations. That was justified both by the low βs (as experimental rotation normally does not exceed the local sound speed) and by the fact that no momentum input for the plasma was present in the system. However, in later years larger βs were achieved, in particular with the use of Neutral Beam Injection (NBI) heating system. In addition to heating the plasma, NBIs also transfer a net momentum to the plasma, which turns into plasma rotation.

One additional area of recent research has been the study of so-called "spontaneous" plasma rotation. This was triggered by the observation of the fact that rotation, up to the order of the plasma sound

speed, is observed in experiments even when no net momentum source exists. That in turn was only allowed by the improvement in plasma diagnostics, which now allow reliable measurements of plasma rotation, both in the toroidal (the long way around the torus) and in the poloidal (the short way around the torus) directions. See for instance Refs. [1, 2] for experimental findings of spontaneous plasma rotation in tokamaks.

Rotation effects are very important for the Spherical Torus [3], where high Mach numbers can be reached. Another area of research where the inclusion of the equilibrium flow is important is the study of Resistive Wall Modes (RWMs). It is known that small changes in dissipation/flow profiles can influence the stability of this branch [4, 5]. The effect of shear flow is also important in reducing plasma turbulence and it has been related to the appearance of the Internal Transport Barrier (ITB) in tokamaks [6] In addition to this, as we will describe in Sec. IV, the inclusion of flow can give a simple explanation of experimental observations made in the RFP devices.

The previous discussion makes it clear that accurate equilibrium calculations are necessary to the progress of the magnetic confinement research, and that plasma rotation should be included in the equilibrium calculation. Only a few codes exist that are capable of calculating equilibria with flow. Among them is the code FLOW [7], on which the rest of this work is focused. FLOW has been used for several years to model various kinds of equilibria in various magnetic configurations. In the present work, we describe some of the latest addition to FLOW, and their application to tokamaks and RFPs.

The remainder of this work is organized as follows. In Section II we briefly summarize the FLOW equilibrium model and code capabilities.

In Section III we describe some applications to several tokamak experimental devices. In Section IV we discuss the extension of FLOW to Reverse Field Pinch (RFP) equilibria.

II Short review of the FLOW code.

FLOW [7] is an equilibrium code solving the Grad-Shafranov-Bernoulli (GSB) system of equations. The equations solved by FLOW are described in [7] and based on the work in [8, 9], and will only be very briefly summarized here. The GSB system is derived from the system of equations including Maxwell's equations and conservation of mass and momentum under the assumption of axisymmetry. The model allows for finite equilibrium flow velocity in both the toroidal and poloidal directions and finite pressure anisotropy in the parallel and perpendicular directions. An additional equation is necessary to close the system (in addition to an equation of state). The closure equation depends on the plasma collisionality and on the anisotropy, since for an anisotropic plasma two equations are necessary, one for each temperature. In FLOW these are the standard ideal MHD closure for isentropic/isothermal flows or the kinetic closure derived from the guiding center constants of motion in the anisotropic case.

By using axisymmetry, Faraday's law and dotting the momentum equation with $\hat{e}_\varphi$, either $\vec{v}$ or $\vec{B}$, and $\nabla\psi$, five (in the isotropic case) or six (in the anisotropic case) integrals of the system are obtained, which are free functions of the magnetic poloidal flux ψ. The free functions used by FLOW, their physical meaning, and their relations to the models of Refs. [8, 9] are listed in Tables I and II of Ref. [7].

For the sake of completeness, we reproduce the equations solved by

4

FLOW, the algebraic Bernoulli equation and the PDE Grad-Shafranov equation. The Bernoulli equation is derived by taking the $\vec{v}$ (or $\vec{B}$) component of the momentum equation, and reads:

$$\frac{1}{2}\left[\frac{\Phi(\psi)B}{\rho}\right]^2 - \frac{1}{2}[R\Omega(\psi)]^2 + W = H(\psi), \tag{1}$$

where $\Phi(\psi)$ is the free function determining the field-aligned flow, $\Omega(\psi)$ the function determining the purely toroidal component of the flow, $W(\rho, B, \psi)$ is the plasma enthalpy and $H(\psi)$ the Bernoulli function. All other symbols have their usual meaning. Equation (1) is solved for the mass density ρ.

The $\nabla\psi$ component of the momentum equation gives the GS equation. Since we will not consider anisotropy in the remainder of this work, we only reproduce the GS equation for isotropic plasmas in the presence of arbitrary flow:

$$\frac{1}{\mu_0}\nabla \cdot \left[\left(1 - M_{Ap}^2\right)\left(\frac{\nabla\psi}{R^2}\right)\right] = -\frac{B_\varphi}{\mu_0 R}\frac{dF(\psi)}{d\psi} - \left(\vec{v} \cdot \vec{B}\right)\frac{d\Phi(\psi)}{d\psi}$$
$$-R\rho v_\varphi\frac{d\Omega(\psi)}{d\psi} - \rho\frac{dH(\psi)}{d\psi} + \frac{\rho^\gamma}{\gamma - 1}\frac{dS}{d\psi}. \tag{2}$$

In Eq. (2), the poloidal Alfvénic Mach number M_{Ap} is given by $M_{Ap}^2 \equiv \Phi^2(\psi)/\rho$, $S(\psi)$ is the entropy, and all remaining symbols are either intuitive or have been defined previously. Details of the definitions can be found in [7, 8, 9].

Recently several diagnostics and post-processing features have been added to FLOW. Many of the diagnostics described in the following are based on integrals on a magnetic surface. Since FLOW is written in Cartesian coordinates, the implementation requires a coordinate transformation, which is performed numerically with standard techniques.

A diagnostic for calculating the fraction of trapped particles has been implemented. For the time being, we have only considered the

5

textbook case of a Maxwellian distribution (due to the difficulty of writing a distribution function giving the MHD plasma characteristics obtained with FLOW). In this case the trapped fraction is given by $f_t(\psi, \chi) = \sqrt{1 - B(\psi, \chi)/B_{MAX}(\psi)}$, where χ is the angle measured along the magnetic surface [10]. Bootstrap current calculations have also been implemented following two approaches [11, 12, 13]. Both the Sauter model (Refs. [11, 12]) and the NCLASS model (Ref. [13]) are based on the Fokker-Planck equation with the full collision operator. In the Sauter model, the neoclassical conductivity is written as the product of the Spitzer conductivity and of an algebraic function of the effective trapped fraction, effective Z and normalized electron collisionality ν_{e*}. The effective trapped fraction is given by:

$$f_t^{eff} = 1 - \frac{3}{4} \langle B^2 \rangle \int_0^{1/B_{MAX}} \frac{\lambda \mathrm{d}\lambda}{\langle \sqrt{1 - \lambda B} \rangle}, \qquad (3)$$

where angular brackets denote an average over the flux surface. Bootstrap current is written in the familiar-looking form:

$$\langle J_\parallel B \rangle_{BS} = -I p_e \left[\mathcal{L}_{31} \frac{p}{p_e} \frac{\partial \ln p}{\partial \psi} + \mathcal{L}_{32} \frac{\partial \ln T_e}{\partial \psi} + \mathcal{L}_{34} \alpha \frac{p_i}{p_e} \frac{\partial \ln T_i}{\partial \psi} \right], \quad (4)$$

where α and the $\mathcal{L}_{3j}$ are coefficients expressed in terms of the effective trapped fraction and collisionality, the subscripts i and e refer to ions and electrons, $I = B_\varphi R$ and the angular brackets denote the average over the magnetic surface. Equation (4) has been implemented in FLOW, using routines analogous to those implemented in CHEASE [14].

The NCLASS model gives a more complicated expression for the bootstrap current, which is also more computationally intense. Without going into the details of the model, which are described in Ref. [13], we will just mention here that the bootstrap current is expressed in terms of the equilibrium macroscopic quantities through the neo-

classical evaluation of particle velocities and dissipative effects. Since a library containing NCLASS equations is freely available, the implementation of that model is straightforward.

The one crucial point that needs additional attention is the possible presence of flow in the equilibrium, which is important for the results in the rest of this work. The Sauter model does not take into account equilibrium rotation. The NCLASS model instead self-consistently includes some neoclassical rotation in its formulation, in the slow-rotation limit. For the time being, we have applied the unmodified Sauter model to equilibria with flow. We have verified that the two models (NCLASS with small rotation and static Sauter) give very similar results in a large number of conditions. We point out that a model taking into account the effect of rotation in a self-consistent way is desirable, but it is not addressed here.

III Tokamak Equilibrium with and without Flow.

We turn now our attention to the effect of plasma rotation on magnetic profiles and bootstrap current in tokamak plasmas. As discussed in Sec. II, five free functions need to be assigned in order to define an equilibrium (in addition to the geometry of the problem). As is well known, those functions are "free" only in the sense that they cannot be determined within the MHD model itself. In order to present meaningful results, we have adopted the following strategy. When experimental data are available, we have used them in our input. For those quantities that cannot be measured, we used in our calculations profiles obtained from static equilibrium reconstructions with standard tools,

such as EFIT or JSOLVER. All data were provided by our colleagues in various institutions that work in closer contact with experiments.

We also point out that to correctly evaluate the effect of rotation, some care is necessary to make sure that all relevant macroscopic quantities (plasma mass, internal energy and current) are conserved when comparing equilibria with different levels of rotation, so that no confusion can arise about the cause of any difference between a static equilibrium and an equilibrium with flow.

We begin our discussion by examining the effect of purely toroidal rotation on the bootstrap current at the 3/2 resonance for three different experiments, the tokamaks JET and DIII-D and the spherical tokamak NSTX. The interest in the plasma properties on the 3/2 resonance is due to the fact that neoclassical tearing modes (NTMs) can develop due to the presence of bootstrap current. Among the three experiments, we expect the effect of rotation to be largest in NSTX, due to its tight aspect ratio and large rotation.

Plasma rotation affects the bootstrap current value at the 3/2 resonance in two ways. First, by modifying the q profile [see Fig. 1(a)] , and thus changing the position of the resonance. Second, by modifying the bootstrap current profile itself [Fig. 1(b)]. In general, we observe that toroidal rotation causes a decrease of the safety factor on axis, as also reported in Ref. [15]. For the cases we have considered, we also observe that the total calculated bootstrap current will decrease slightly in the presence of toroidal rotation (see for example Fig. 4).

For our calculations, we used data for low-β equilibria for the tokamaks ($\beta_t < 4\%$ for both discharges) and high-β for the spherical tokamak ($\beta_t \sim 23\%$). The toroidal beta $\beta_t = 2 < p > /B_V^2$ is defined using the average pressure and the vacuum field. For the tokamaks,
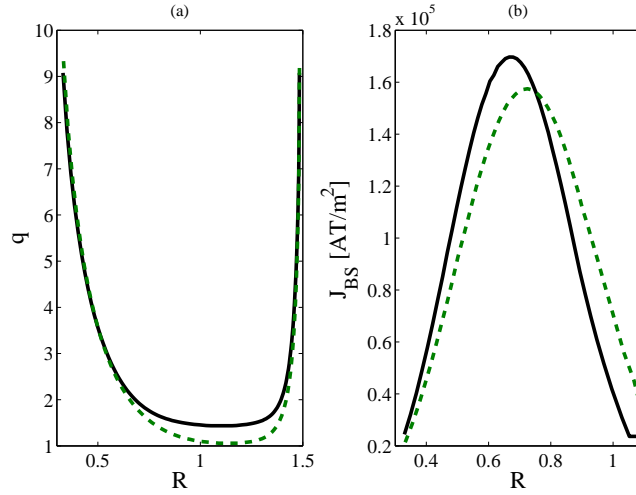
Figure 1: Safety factor profile (left) and bootstrap current profile (right) for a static equilibrium (black) and an equilibrium with about half-sonic rotation (green, dashed). For clarity, only the inboard part of the equilibrium is shown on the right.

experimental rotation profiles were available, as well as experimental density profiles. The low β allowed us to use the experimental profiles with various levels of rotation, since the macroscopic quantities that need to be constant in the different equilibria are only marginally affected by the plasma rotation. For NSTX, we used a quasi-density profile $\sim \sqrt{\psi}$ and a toroidal frequency profile approximately linear in ψ. Both profiles roughly compatible with experimental measurement (see Ref. [7] for the definition of quasi-density and its relation to the density). Note that ψ in FLOW is zero at the edge and maximum on the magnetic axis. This choice of profiles preserves the relevant macroscopic quantities with flow levels up to the highest rotation we considered, with Mach number ~ 0.5.

For each tokamak we ran a few equilibria (three in the JET case, four in the DIII-D case) with different levels of rotation. First, we considered static equilibria, in which we simply ignored the rotation. Next we calculated equilibria with the nominal level of rotation, i.e. with the experimental toroidal frequency. Since both equilibria had a relatively low maximum Mach number, we then repeated the equilibrium calculations with a rotation level twice as large as the experimental one. For the DIII-D discharge, we also used an $\Omega(\psi)$ three times as large as the nominal one. For NSTX, we calculated three equilibria, with maximum toroidal Mach numbers $M_\varphi = v_\varphi / C_s \sim 0.25$ and 0.5. The results are
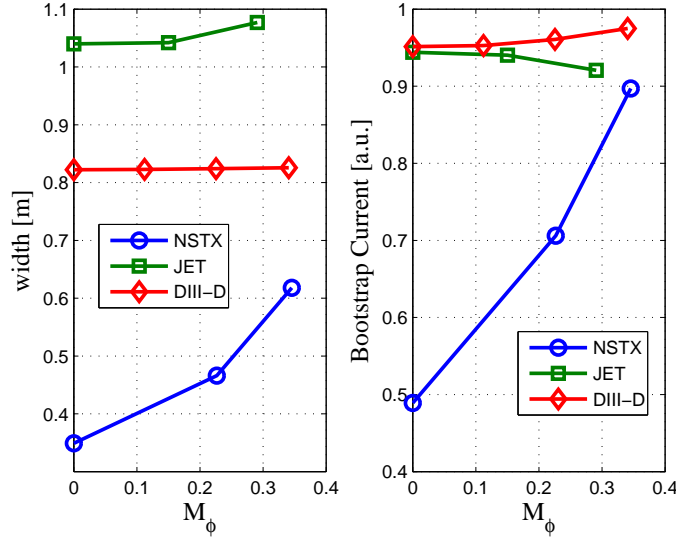

Figure 2: Width of the 3/2 resonant surface in meters (left) and bootstrap current density in arbitrary units (right) for NSTX (blue, circles), JET (green, squares) and DIII-D (red, diamonds) as a function of the toroidal Mach number at the resonant surface.

summarized in Fig. 2. In the left part of the figure, the width of the 3/2

10

resonant surface along the midplane is shown. On the right, the value of the bootstrap current at the resonant surface is plotted in arbitrary units. Both plots show results as a function of the toroidal sonic Mach number measured at the resonant surface. Even though the rotation profiles are different for the three experiments, all of them have rotations increasing from the edge to the plasma center in comparable ways (not shown). For that reason, the local Mach number seemed a fair indicator of the total level of rotation. The resonant surface width was selected as an indicator of the change in the magnetic properties of the equilibrium. It is clear that more information is required to gain a complete understanding of the variation in the equilibrium due to the flow. For instance, one should take into account the fact that the resonant surface is also influenced by plasma shape, and therefore a change in width along the midplane also corresponds to a change in dimension along Z and possibly to a displacement of the whole resonant surface. Nevertheless, the width change is a fair indicator of how much the magnetic geometry is affected by the rotation. Finally, the bootstrap current density levels at the resonant surface were normalized separately for each experiment, in order to be able to show them on the same plot. Each value was normalized to the maximum value of J_{BS} obtained by our post-processor for the corresponding experiment. What should be considered is the relative variation of J_{BS} from the static case to the case with flow. As expected, only small variations (of the order of a few %) are observed in the tokamak case, for both the resonant surface size and the bootstrap current at resonance. On the other hand, large variations in the spherical-tokamak case are observed. The inter-machine comparison is clearly an implicit scansion in β (and aspect ratio). We also performed explicit β scans, both by con-

11

sidering equilibria relative to shots at different betas and by rescaling the pressure profile in the input of FLOW. The physical intuition that an increase in β causes an increase in bootstrap and total current, and a decrease in q_{min}, for tokamaks and spherical tori alike was confirmed numerically. It is important to observe that regardless of β, the effect of toroidal rotation is qualitatively similar to what shown in Fig. 1.

Other factors can influence bootstrap current and q profiles. In particular, we focus on the effect of shaping, examining in detail the effect of changes in the triangularity δ for NSTX equilibria. In order to
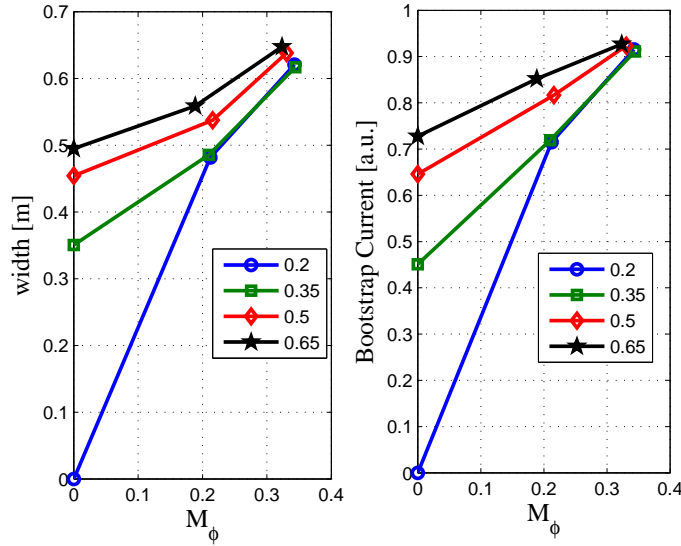

Figure 3: Width of the 3/2 resonant surface in meters (left) and bootstrap current density in arbitrary units (right) for NSTX with different upper triangularities, as a function of the toroidal Mach number at the resonant surface.

do that, an NSTX equilibrium similar to the one presented in Figs. 1 and 2 was considered. The plasma shape was assigned analytically and

modified in a series of equilibria, while leaving the input free functions profiles unchanged. The plasma shape corresponds to a lower single null equilibrium. Only the upper triangularity was modified. The effect of triangularity for $0.2 \leq \delta_u \leq 0.65$ is presented in Fig. 3, where the width of the 3/2 resonance (left) and the bootstrap current at the resonance (right) are plotted as function of the Mach number on the resonance. In this case the effect of triangularity is rather dramatic. That is due to the fact that the safety factor profile is flat near the axis, so that small variations in the equilibrium (and thus in q_{min}) can produce large variations in the position of the resonance. Notice that this is not an artifact, but a typical occurrence in NSTX equilibria. The results in Fig. 3 can be qualitatively explained as follows. An increase in δ causes a decrease in plasma surface. Since the free functions are not modified, the decrease in surface will cause an increase in gradients, and ultimately leads to a lower q_{min}. The reduction in plasma surface dominates the variations in integrated quantities, resulting in a decrease of plasma current and β_t in the case of larger triangularities (since in this case free functions are conserved, rather than integrated quantities). The triangularity variation causes minimal changes in the bootstrap current profile itself; the large variation of the bootstrap current at the resonance is largely due to the q profile change.

Beside the effect of the flow magnitude it is also important to analyze the effect of flow shear. In order to do that, we consider a series of rotation profiles with an increasingly sharper variation at some selected value of ψ. The series of profiles is shown for an NSTX equilibrium with $M_\varphi \sim 0.5$ in the left pane of Fig. 4. The sharp gradient has been placed at the 3/2 resonance. The blue curve corresponds to the smooth profile used for the calculation presented in Fig. 2. The right
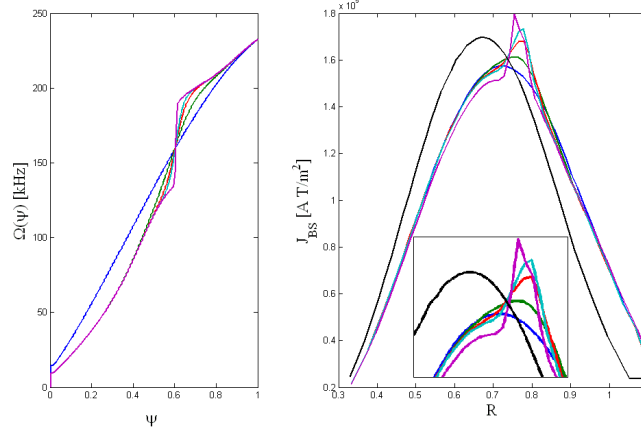
13

Figure 4: Toroidal rotation frequency (left) and bootstrap current (right). Equal colors correspond to the same equilibrium. The static bootstrap current profile is shown for reference (in black). A zoom of the region with sharp velocity variation is also shown.

pane of Fig. 4 shows the bootstrap current profiles for the various rotation profiles, with same colors referring to the same profile. The static bootstrap current curve is also shown (in black) for reference. The insert shows a zoom of the resonance region. For clarity, only the region inboard of the magnetic axis is shown. The current profiles become increasingly more discontinuous as the rotation profiles acquires sharper gradients. This can be explained qualitatively observing that a sharp variation in the rotation profile will also cause a sharp variation in the density profile, due to Eq. (1), which in turn produces a sharp variation in pressure and temperature, and thus in the bootstrap current profile, due to Eq. (4). Note that the safety factor profile is essentially identical for all equilibria presented in Fig. 4 (not shown). We have also investigated the effect of flow shear on other equilibria

14

(for tokamaks, with smaller rotations, and for a different position of the discontinuity), and verified, as was expected, that the effect of flow shear, although qualitatively consistent, is largest for larger flows and for high-β and tight aspect ratio. Note that the profiles with the sharpest gradients are possibly not very realistic: they have been used only to emphasize the effect of flow shear. However, it should be noted that strong toroidal flow velocity shear generates sharp gradients in density and temperature profiles, features that are similar to what is for example observed in ITB plasmas.

One additional subject of interest is the effect of poloidal rotation on the magnetic and bootstrap current profiles. Experimental measurements of poloidal flow velocity are less common and less accurate than measurements for toroidal rotation. That is in part due to the fact that measurements rely on an indirect calculation of the radial electric field through impurity rotation measurements.

In order to gain at least some insight on the effect of subsonic poloidal rotation, we have computed a series of equilibria with different levels of rotation for all three machines considered in the previous discussion. Since it is commonly acknowledged that poloidal rotation vanishes in the plasma core, we have chosen for each machine a rotation profile with a non-zero velocity (approximately constant for each machine) at the plasma edge, a maximum velocity inside the plasma, and zero velocity in the core. In order to limit the poloidal rotation to the edge region of the plasma, the maximum was assigned to coincide with the $q = 2$ surface, and a value of about $\simeq 30km/s$, loosely compatible with experimental observations [16] was chosen. Finally, the rigid toroidal rotation was minimized, in order to focus on the effect of poloidal flow.

Due to the small velocities involved, direct calculation shows that poloidal flow only marginally modifies the equilibrium. As in the case of toroidal rotation, the maximum effect is observed in the highest beta machine, i.e. NSTX. This is due in part to the fact that the $q = 2$ surface in NSTX is the one that is largest compared to the minor radius of the plasma, meaning that in the NSTX case a larger fraction of the plasma is spinning in the poloidal direction, compared to the other machines. The effect of the poloidal rotation on the q profile is small. The only area considerably affected is the one next to the $q = 2$ resonance (maximum of poloidal velocity), where the magnetic shear has a clear, even if small, increase with increasing rotation. The NSTX equilibrium with largest velocity has a peak bootstrap current value about 8% larger than the static value. The total bootstrap current, as well as the total plasma current increase by less than 2%. The local variation is explained by the fact that in the NSTX case the maximum of J_{BS} is very close to the $q = 2$ surface, and by the variation in the density, pressure and temperature profiles in the higher-flow region, due to the effect of rotation on the solution of Eq. (1). Due to a combination of the lower β and of the different bootstrap current profiles, the effect of poloidal rotation on the examined JET and DIII-D equilibria is instead negligible.

We now move to the study of Reversed Field Pinch equilibrium.

IV   Reversed Field Pinch Equilibrium

FLOW has also been modified to study axisymmetric Reversed Field Pinch (RFP) equilibrium. Before entering in to the detail of FLOW RFP equilibria, we note that FLOW two-dimensional representation

of RFPs does not take into account the three-dimensional part of the RFP dynamics. Reversed Field Pinches are inherently 3D objects with strong helical character, so our description of the RFP equilibrium is per force an approximation. Nevertheless, some interesting results are already obtained in the axisymmetric approximation, as is described in the remainder of this Section.

The main difference between a tokamak and an axisymmetric RFP equilibrium from the point of view of a numerical solution is that the toroidal component of the magnetic field changes sign on some magnetic surface, the so-called reversal surface. A vanishing toroidal field does not constitute a problem for FLOW, which has in fact been used in the past to model equilibria with purely poloidal magnetic field [17]. In the present Section, we first discuss the RFP FLOW implementation and the equilibrium results, and then turn our attention to the neoclassical results obtained with the new diagnostics. Even though FLOW can compute transonic equilibria, the discussion in the present work is restricted to subsonic poloidal rotations.

IV.1 RFP Equilibrium with flow.

The input for FLOW in the case of RFP equilibria is essentially identical to the input for a tokamak case, with the only difference that the free function $F(\psi)$ changes sign inside the plasma in the case of a reversed equilibrium. We recall here that the toroidal field is given by:

$$B_\varphi = \frac{1}{R} \frac{F(\psi) + \mu_0 R^2 \Phi(\psi)\Omega(\psi)}{1 - \Phi^2(\psi)/\rho}. \tag{5}$$

We observe that in the static case B_φ will change sign on the same magnetic surface where $F(\psi)$ does. However, in the presence of rotation the second term of the numerator in Eq. (5) in general does not

vanish. That means that in the presence of flow the reversal surface does not need to be a magnetic surface.

In order to investigate the issue and also to make FLOW more useful to the RFP community, the model proposed in Ref. [18] was implemented in the code, giving:

$$F(\psi) = F_0 \left[1 + \mu \left(\psi - 1 + \frac{(1 - \psi)^{k+1}}{k + 1} \right) \right].$$

(6)

This is the profile typically used in axisymmetric-RFP modeling. For convenience, the poloidal flux ψ is here normalized to be one in the center and zero at the plasma edge. All other equilibrium characteristics relevant to RFPs can be easily inserted in FLOW, for instance the so-called "pancake" profile for the temperature [19] (which is, of course, inserted through the quasi-pressure and quasi-density profiles).

The effect of Eq. (5) on field reversal was verified with numerical results for equilibria with both toroidal and poloidal rotation, with both $\Omega(\psi) \neq 0$ and $\Phi(\psi) \neq 0$ where $F(\psi) = 0$. Direct calculation shows that for free functions profiles compatible with measurements in RFX-mod the $B_\varphi = 0$ curve is only slightly different from a magnetic surface. If one considers the magnetic surface that is tangent to the $B_\varphi = 0$ surface on the inboard side of the plasma, the two surfaces move apart as one moves toward larger R, with the maximum distance between the two occurring on the outboard side of the plasma. We have verified that for realistic pressure, density, rotation and toroidal field profile (as referred to RFX-mod) the maximum distance is of the order of a few ‰ of the minor radius of the plasma. Since the difference is so small, it will not be discussed any further in the present work. It is however possible that for future machines flow will play a larger role in determining the reversal surface.

We now turn our attention to the velocity profiles. The expression

for the two components of the plasma velocity:

$$\vec{v}_p = \frac{\Phi(\psi)}{\rho}\vec{B}_p, \qquad v_\varphi = \frac{\Phi(\psi)}{\rho}B_\varphi + R\Omega(\psi), \tag{7}$$

shows that if the plasma is rotating in the poloidal direction a toroidal component of the velocity is also present. This is actually a more general result than what is expressed by Eq. (7) [20]. In the case of reversal, there is an additional remarkable effect of Eq. (7). If $\Omega(\psi) = 0$ and the flow extends across the reversal surface, then either the poloidal or the toroidal (but not both) component of the velocity must change sign at the reversal. We have considered a set of equilibria where $\Phi(\psi)$
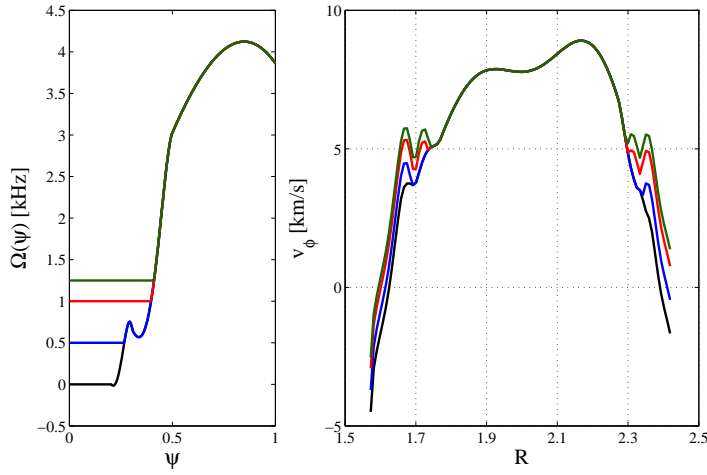

Figure 5: Input $\Omega(\psi)$ (left) and toroidal velocity (in km/s) of a reversed RFP equilibrium (right). Same colors correspond to the same equilibrium.

remains positive across the reversal, and different constant values are used for $\Omega(\psi)$ in the edge region, using data typical for the Reversed Field Experiment in Padua [21]. In assigning the free functions determining plasma rotation, we relied on the available experimental measurements. Since no information is available on the rotation profile in

19

the central part of the plasma, we assign the free functions Φ and Ω in Eq. (7) in order to have a roughly constant toroidal rotation in the core region. Edge measurements [22] show velocities in the range of a few km/s, similar to the ones in Fig. 5. The resulting equilibria are presented in Fig. 5, showing that the toroidal component of the velocity changes sign. The position of the flow reversal changes depending on the edge value of $\Omega(\psi)$. Indeed, it is possible for the flow to reverse only in part of the edge region. That is highlighted by the equilibria with larger edge Ω (red and green curve in Fig. 5), which reverse on the inboard side of the plasma, but not on the outboard side. This is an important effect, which arises from the self-consistent treatment of equilibrium with flow in RFPs. A possible future enhancement of the presented results could be obtained with a direct comparison of the local transport model and of the MHD equilibrium predictions, since more detailed transport calculations or measurements are required to determine the correct edge value for $\Omega(\psi)$. We point out that available experimental observations suggest that rigid toroidal rotation at the plasma edge should be small, since $\Omega(\psi) \simeq 0$ in Eq. (7) is required to obtain flow reversal next to the field reversal. We have shown that flow reversal does not necessarily occur on the same surface as field reversal, which is located around $r/a = 0.875$ in the equilibria in Fig. 5. Note that the slightly "bumpy" character of the profiles in Fig. 5 is due to the varying contribution along the profile of the different functions that determine the velocity, and has no particular meaning. Due to our choice of free functions, the poloidal velocity is finite in the edge region of the plasma, but does not change sign (not shown).

IV.2 Bootstrap Current and Neoclassical Resistivity in RFP equilibria.

Preliminary result for bootstrap current and neoclassical resistivity calculations in RFP systems have been already presented [23].

The first consideration that needs to be made with respect to neoclassical calculations in RFPs using the available tools is that the results of Refs. [11, 12, 13] can be directly applied to RFPs. That is because in their derivation, no assumption is made on the scaling of the fields, which is the main difference between tokamaks and RFPs ($B_\varphi >> B_\theta$ vs. $B_\varphi \simeq B_\theta$).

It was shown in Ref. [23] that the bootstrap current fraction is rather small in realistic RFP configurations, too small in fact to give any meaningful contribution to the total plasma current. Even so, we want to extend the analysis to recently achieved plasma configurations at high current. The two equilibria shown in Fig. 6 were used in the study. The first equilibrium, which is labeled as "pancake" in the figure, approximates the temperature profile that is observed in high-current RFX-mod discharges, with a hot core region and a colder edge region, with the transition between the two occurring with a sharp gradient. The second equilibrium, labeled as "flat" in the figure, corresponds to a more traditional temperature profile, smoothly increasing from the edge to the plasma center. The "pancake" equilibrium, proposed as a schematic approximation of the so-called SHAX state [19] is observed in Quasi-Single-Helicity (QSH) regimes in RFX-mod, and is a very interesting new feature in RFP physics [24]. These regimes are commonly observed in RFX-mod when plasma current is above $I_p \gtrsim 1\ MA$, and present significant chaos reduction with the appearance of clear transport barriers. Since FLOW is a one-fluid code, the
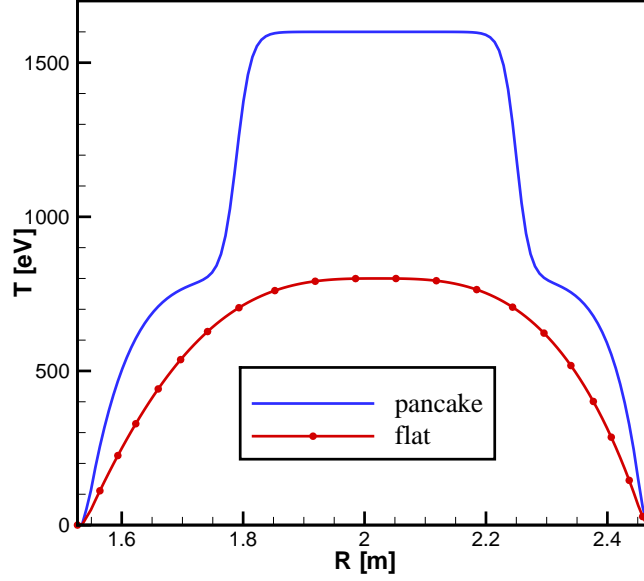
Figure 6: Temperatures in $[eV]$ along the midplane for two RFP equilibria.

plotted temperature is the total temperature, $T = T_i + T_e$. Both equilibria have the same density profile and reversed toroidal field (not shown). In this case, the purpose is to study the effect of increasing temperature/pressure on the bootstrap current profile. For that reason, we purposely did not try to keep constant the quantities that were kept constant in the tokamak discussion in Section III. At any rate, since the plasma β is small, plasma current is essentially the same, $I_p \sim 1MA$ for both equilibria, even though β is rather different, with the poloidal β β_p equal to about 6% for the "pancake" profile and about 3.5% for the "flat" equilibrium.

The bootstrap current profiles for the two equilibria are shown in Fig. 7. As was done before, the bootstrap current was normalized to
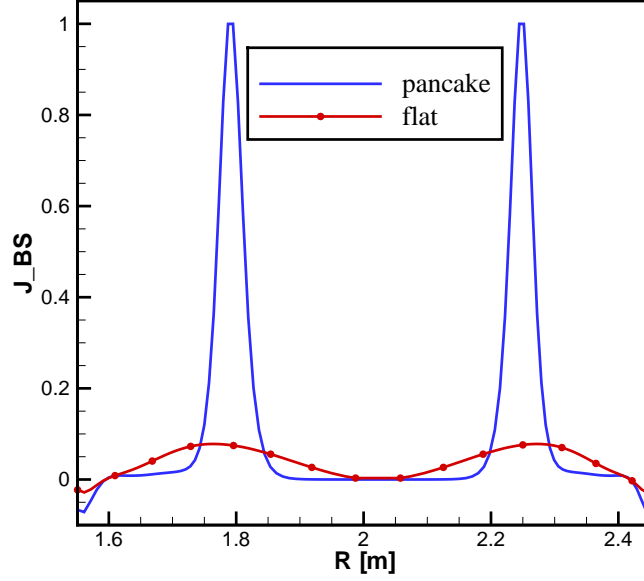
22

Figure 7: Bootstrap current profile for two RFP equilibria, in consistent, arbitrary units.

its maximum calculated value. Both curves were normalized to the maximum value of the equilibrium with larger current, the "pancake" equilibrium. Note that the current in the "flat" equilibrium is only a small fraction of the current in the "pancake" equilibrium. Both curves peak where the corresponding temperature gradients are largest, as can be inferred by comparing Fig. 6 and Fig. 7. It can also be observed that both curves change sign close to the plasma edge. In both equilibria the bootstrap current is, however, only a small fraction of the total current, with the maximum bootstrap fraction $f_{BS}^{Max} \simeq 1\%$ for the "pancake" case and $f_{BS}^{Max} \simeq 0.1\%$ for the "flat" case. Due to the increase in bootstrap fraction as effect of increasing temperature, one can expect

23

bootstrap current to play a larger role in the future, especially if higher temperatures and temperature gradients are obtained in experiments. Still, with the RFX-mod-relevant profiles used in our study, it does not seem likely that bootstrap fractions close to unity, as those described in Ref. [25], can be obtained.

We have also investigated the effect of rotation on the bootstrap current profiles, as was done in Section III for tokamaks. Since β is relatively low and the velocities are also low (measured toroidal velocities do not exceed 50 km/s in RFX-mod), plasma rotation has a small effect on bootstrap current profiles, and can be ignored in that respect for all practical purposes.

As a final note, we point out that in the edge region of the plasma, where the toroidal field is small or zero, the parallel current is in the poloidal direction. That also applies to the bootstrap current, which is mainly in the poloidal direction at the plasma edge. This is a difference with respect to the tokamak, where the toroidal field is everywhere considerably larger than the poloidal field, and therefore the parallel current is always mostly in the toroidal direction.

As a last topic in this Section, we turn our attention to neoclassical resistivity profiles. Being the RFP an ohmic device the determination of the corrections (including neoclassical) to the classical Spitzer's resistivity is of fundamental importance in order to clarify the scalings and in order to compare more carefully experimental data with theoretical predictions.

The discussion in Ref. [23] is extended here to consider the effect of different equilibrium properties on the neoclassical resistivity. We have applied Sauter's model to the calculation of neoclassical resistivity for both the "pancake" and the "flat" equilibria. Since the
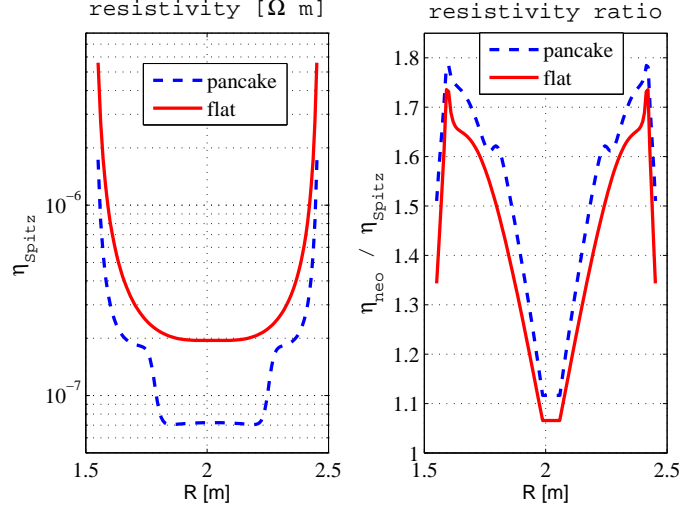
Figure 8: Spitzer resistivity in $[\Omega m]$ for two RFP equilibria (left) and ratio between neoclassical and Spitzer resistivity (right).

neoclassical resistivity is expressed in terms of Spitzer's resistivity, we have also calculated profiles for the Spitzer resistivity for comparison. The neoclassical resistivity value depends on the Z_{eff} (effective Z) profile. Consistently with the results of experimental measurements, we set the profile for Z_{eff} as:

$$Z_{eff} = Z_0 + \delta Z \left(\frac{\psi}{\psi_c}\right)^{\lambda}, \tag{8}$$

with $Z_0 = 1$, $\delta Z = 1.5$ and $\lambda = 0.25$. Note that Z_{eff} is not measured directly in RFX-mod experiments, and that the profile in Eq. (8) is a reasonable profile often used in experiment modeling. The main results of our calculation are showed in Fig. 8. In the left part of the figure, the Spitzer resistivity profiles for the two equilibria are shown. As expected, resistivity is lower in the "pancake" equilibrium, due to its higher temperature, and both resistivity profiles closely follow

25

the temperature profiles in Fig. 6. More interesting is the effect of neoclassical terms on the resistivity value, shown in the right part of the figure. Neoclassical resistivity is everywhere higher than classical resistivity, and its profile depends on plasma collisionality and Z_{eff}. The two profiles shown in the right pane Fig. 8 are rather similar. That is due to the fact that the same Z_{eff} and density profiles has been used for both curves, and to the fact that collisionality for the two equilibria are rather similar, at least qualitatively. The sharp transitions close to the plasma edge are due to the variation in temperature, which sharply decreases. In this cold plasma region the collisional detrapping has a large effect, which in our model is accounted for by the effective trapped fraction. As can be seen from Fig. 8 in that region the neoclassical resistivity becomes very close to the classical one.

V   Summary and Conclusions

In the present work, we have described applications of the equilibrium code FLOW to tokamak and reversed field pinch simulations.

New features and neoclassical effects calculations using the Sauter and NCLASS models have been implemented in FLOW.

The first outcome of our work is to have positively benchmarked the two models.

In the application of neoclassical calculations to tokamak equilibria, it was shown that due to equilibrium flow the change in magnetic and bootstrap current profiles could in principle have a large effect on the stability of resonant modes such as NTMs, at least for high-β, small aspect ratio devices such as the spherical tokamak NSTX. Moreover, the inclusion of the equilibrium flow produces in NSTX-like equilibria

an appreciable displacement of the resonance surface of NTMs. This may have an implication for the active control of the modes, which requires a precise deposition of the radiofrequency at the island O-point. Another consequence is for theoretical studies of NTMs and comparison with experimental data in Spherical Tokamaks (e.g. by using the standard Rutherford model).

A strong toroidal flow shear near the resonance can cause a large variation in the bootstrap current profile, and therefore also influence the evolution of NTMs. Regarding poloidal flow we have shown that it is too low in experiments to affect the equilibrium. We also applied FLOW to axisymmetric RFP calculations. We showed the effect of field reversal on plasma velocity, in particular on velocity reversal. This is an interesting effect, which can explain experimental observations of the flow structure in the RFX-mod plasma edge [22]. The precise location of the velocity null point is affected by the amount of flow at the plasma edge. It coincides with the toroidal field null for cases with vanishing edge rigid toroidal rotation. Then, we discuss the issue of bootstrap current in RFPs equilibria, showing that for realistic data (relative to present-day experiments) only a minimal amount of bootstrap current is present. Very different results were presented in previously published work [25], possibly because of very different (and in our opinion quite unlikely) assumptions on βs and current profiles. For realistic profiles the local maximum bootstrap current fraction ranges from 0.1 to 1 % in present devices. Finally we described how the resistivity profile is modified by neoclassical effects, showing that the neoclassical resistivity can exceed the classical Spitzer value by up to a factor of two. Moreover, the neoclassical effects are further modified taking into account collisions, which can detrap particles: a

non negligible effect, particularly at the cold plasma edge.

In conclusion, taking into account the equilibrium plasma flow in different magnetic confinement systems can help in understanding the phenomenology observed in experiments, in interpreting measurements and may also help the active control of MHD instabilities, since, as we have shown for high-β plasmas, the mode resonance radii can be largely affected by plasma flow.

In general, it is appropriate to keep into account the equilibrium modifications due to plasma rotation in stability studies. With modern codes, the additional level of complication required to do that is almost negligible, and is not sufficient reason to ignore rotation in the equilibrium. As shown here the effect of flow can be large or even subtle but in every case it has an effect that can be, in our opinion, very important as far as stability is concerned, not only indirectly (for example through wave dumping mechanisms)but also directly, by modifications of q, current, density and or temperature profiles.

VI   Acknowledgments.

References

[1] RICE, J. E., INCE-CUSHMAN, A. C., REINKE, M. L., et al., Plasma Physics and Controlled Fusion **50** (2008) 124042 (11pp).

[2] DUVAL, B. P., BORTOLON, A., KARPUSHOV, A., et al., PHYSICS OF PLASMAS **15** (2008).

[3] ONO, M., KAYE, S., PENG, Y.-K., et al., Nucl. Fusion **40** (2000) 557.

[4] GAROFALO, A. M., JACKSON, G. L., LA HAYE, R. J., et al., Nucl. Fusion **47** (2007) 1121.

[5] STRAIT, E. J., GAROFALO, A. M., JACKSON, G. L., et al., Physics of Plasmas **14** (2007) 056101.

[6] TALA, T., ANDREW, Y., CROMBE, K., et al., Nuclear Fusion **47** (2007) 1012.

[7] GUAZZOTTO, L., BETTI, R., MANICKAM, J., and KAYE, S., Phys. of Plasmas **11** (2004) 604.

[8] HAMEIRI, E., Phys. Fluids **26** (1983) 230.

[9] IACONO, R., BONDESON, A., TROYON, F., and GRUBER, R., Phys. Fluids B **2** (1990) 1794.

[10] FREIDBERG, J. P., *Plasma Physics and Fusion Energy*, Cambridge University Press, Cambridge UK, 2007.

[11] SAUTER, O., ANGIONI, C., and LIN-LIU, Y. R., Phys. of Plasmas **6** (1999) 2834.

[12] SAUTER, O., ANGIONI, C., and LIN-LIU, Y. R., Phys. of Plasmas **9** (2002) 5140.

[13] HOULBERG, W. A., SHAING, K. C., HIRSHMAN, S. P., and ZARNSTORFF, M. C., Phys. of Plasmas **4** (1997) 3230.

[14] LÜTJENS, H., BONDESON, A., and SAUTER, O., Comput. Phys. Commun. **97** (1996) 219.

[15] HOLE, M. J. and DENNIS, G., PLASMA PHYSICS AND CONTROLLED FUSION **51** (2009).

[16] AUSTIN, M. E., BURRELL, K. H., WALTZ, R. E., et al., Physics of Plasmas **13** (2006) 082502.

[17] GUAZZOTTO, L., FREIDBERG, J. P., and KESNER, J., Phys. of Plasmas **14** (2007) 062501.

[18] PACCAGNELLA, R., BONDESON, A., and LÜTJENS, H., Nucl. Fusion **31** (1991) 1899.

[19] LORENZINI, R., TERRANOVA, D., ALFIER, A., et al., Phys. Rev. Lett. **101** (2008) 025005.

[20] THROUMOULOPOULOS, G. N., WEITZNER, H., and TASSO, H., Phys. of Plasmas **13** (2006) 122501.

[21] ROSTAGNI, G., Fusion Eng. Des. **25** (1995) 301.

[22] ANTONI, V., DESIDERI, D., MARTINES, E., SERIANNI, G., and TRAMONTIN, L., Phys. Rev. Lett. **79** (1997) 4814.

[23] GOBBIN, M., GUAZZOTTO, L., GUO, S. C., et al., *to appear in* Journal of Plasma and Fusion Research Series (2008).

[24] CAPPELLO, S., Theory of Fusion Plasma Conference, Varenna (2008).

[25] SHIINA, S., NAGAMINE, Y., TAGUCHI, M., et al., Phys. of Plasmas **12** (2005) 080702.